



Investigation on Compressibility and Microstructure Evolution of Intact Loess at Different Wetting States

Tao Jian^{1,2}, Lingwei Kong¹, Wei Bai^{1*} and Zhiliang Sun¹

¹State Key Laboratory of Geomechanics and Geotechnical Engineering, Institute of Rock and Soil Mechanics, Chinese Academy of Sciences, Wuhan, China, ²University of Chinese Academy of Sciences, Beijing, China

Loess is widely deposited in arid and semi-arid areas and is characterized by low dry density, developed pore space, and loose structure, which is not commensurate with high structural strength and shear strength in the dry state. Many natural phenomena and experimental results show that intact loess is very sensitive to the change of water content, and a slight increase in water content can cause a rapid reduction in strength. Abundant information is available in the literature for the collapsibility of loess. However, research on the evolution of loess compressibility during wetting, which is very helpful in understanding loess collapsible deformation caused by long-term irrigation, remains minimal. To this end, in this article, the evolution of the compressibility of intact loess at different wetting stages is investigated by oedometer tests, and microstructure and pore size distribution (PSD) were characterized on intact loess specimens at different water contents before and after oedometer tests by scanning electron microscope (SEM) and mercury intrusion porosimetry (MIP) methods. The results show that the compression index (C_c) and secondary compression index (C_{α}) of intact loess depend on water content and vertical stress and change abruptly when vertical stress exceeds yield stress. C_{α}/C_c values of intact loess are not constant, which increases with vertical stress to a peak and then gradually decreases to 0.025. Wetting and loading can cause damage to the microstructure of intact loess; specifically, loading leads to the collapse of the overhead structure and the transformation from a bimodal PSD into a unimodal PSD, and wetting intensifies the collapse of the microstructure to form a compacted interlocking structure and promotes the transformation of medium pores into small pores.

OPEN ACCESS

Edited by:

Zetian Zhang,
Sichuan University, China

Reviewed by:

Xiaolin Weng,
Chang'an University, China
Li Wang,
Xi'an University of Science and
Technology, China

*Correspondence:

Wei Bai
wbai@whrsm.ac.cn

Specialty section:

This article was submitted to
Geohazards and Georisks,
a section of the journal
Frontiers in Earth Science

Received: 19 April 2022

Accepted: 23 May 2022

Published: 01 July 2022

Citation:

Jian T, Kong L, Bai W and Sun Z (2022)
Investigation on Compressibility and
Microstructure Evolution of Intact
Loess at Different Wetting States.
Front. Earth Sci. 10:923358.
doi: 10.3389/feart.2022.923358

Keywords: intact loess, water content, compressibility, microstructure, SEM, MIP

1 INTRODUCTION

Loess is aeolian sediment in arid and semi-arid areas, which is widely distributed in Africa (Nouaouria et al., 2008), South America (Francisca, 2007), North America (Saye et al., 1988), Europe (Bally, 1988), Oceania (Yates et al., 2018), and Asia (Youssef and Maerz, 2013; Sadeghi et al., 2019; Zhang et al., 2019), especially in the Loess Plateau of China, with continuous distribution and enormous thickness (Liu, 1985). The unique material composition, depositional environment, and depositional mode have resulted in a weakly cemented, highly porous metastable structure of loess, which is characterized by aggregate particles and overhead structure. The metastable structure has a decisive role in the collapsibility and compressibility of loess when wetted and loaded (Gao, 1988;

Assallay et al., 1997; Li et al., 2016). Natural loess at a low water content has high strength and remains stable; however, even if wetted slightly, its strength decreases sharply, resulting in the destruction and collapse of the structure under loading, not to mention inundated (Wen and Yan., 2014; Yates et al., 2018). Numerous geological disasters in the loess area are closely related to the great deformation caused by wetted loess, such as differential settlement (Hou et al., 2019), earth cracks (Lu et al., 2019), and destruction of infrastructures (Bally, 1988; Saye et al., 1988). With the development of society, increasing human activity in the Loess Plateau will bring about more potential problems of loess collapse caused by wetting. Among them, long-term irrigation is the most important factor for the frequent occurrence of geological disasters (such as landslide and land subsidence) in the loess tableland (Juang et al., 2019). However, compared with landslides (Xu et al., 2014; Leng et al., 2018), literature concerning land subsidence caused by long-term irrigation is very limited (Hou et al., 2019).

Since the last century, geotechnical practitioners and researchers have studied the problem of collapsible deformation of loess due to wetting. Many researchers proposed the method of measuring the collapsibility coefficient by the double oedometer and soaking triaxial test (Reznik, 1992; Jiang et al., 2012), summarized the relationship between soil physical and mechanical properties and collapsibility (Handy, 1973; Grabowska-Olszewska, 1989; Francisca, 2007; Sadeghi et al., 2019; Zhang et al., 2019), suggested the prediction model of loess collapsibility (Xie et al., 2018; Hou et al., 2019), clarified the collapsible mechanism based on the mineral composition and microstructure of loess (Barden et al., 1973; Dijkstra et al., 1995; Assallay et al., 1997; Smalley and Marković, 2014; Li et al., 2016; Liu et al., 2016), and estimated collapsibility deformation in the field through the loess collapsibility coefficient measured in the laboratory (Shao et al., 2015). The works reported in literature focused on the characteristics and mechanism of the instantaneous collapse of loess during inundating. However, accurately estimating the loess settlement deformation caused by long-term irrigation based on the results of the loess collapse test in laboratory is difficult. The main reasons are as follows: 1) within the influence range of irrigation infiltration, the water content of the soil increases, but the soil is nearly saturated only in the surface layer (Hou et al., 2018). 2) Changes in soil properties caused by the development of wetting deformation are observed. 3) This process is long term, and the secondary compression of soil should not be ignored. Therefore, to estimate the settlement deformation due to long-term irrigation accurately, a better understanding of the evolution of the compressibility of intact loess during wetting is required. Limited information is found in literature for the wetting deformation of loess, which introduces the relationship between the wetting deformation coefficient and influencing factors (such as vertical stress, properties of loess, and wetting water content) and only for remolded loess (Yang et al., 2017).

The microstructure remarkably affects the hydro-mechanical behavior of loess. However, the evolution of the microstructure of loess during wetting and loading remains unclear. The evolution

information of loess microstructure under wetting and loading helps to better understand the compression deformation characteristics of loess and provides a solid basis for the constitutive model that can better fit the hydro-mechanical behavior of loess (Wang et al., 2018; Wang et al., 2020). Particle pattern, contact relation, bonding material, and pore size distribution (PSD) are the key factors of metastable loess microstructure, and accurately characterizing them is important for understanding the deformation of loess due to wetting (Gao, 1980a; Gao, 1980b; Li et al., 2016). A scanning electron microscope (SEM) is commonly used to observe the microstructure of soil, thus playing an important role in observing the particle morphology, interparticle cementation, and size and shape of the pore. In addition, the SEM images are processed by image processing software to acquire the quantitative information of microstructure (Li and Li, 2017; Li et al., 2019), but this work is extremely cumbersome and involves some subjective judgments on the distinguishing between particles and pores (Li et al., 2016; Wang et al., 2018; Wang et al., 2020). Mercury intrusion porosimetry (MIP) is a reliable technique for measuring pores of the soil. Although the original structure of loess may be destroyed during the early intrusion, many studies have successfully measured the PSD of loess using the MIP method (Lei, 1987; Jiang et al., 2014; Ng et al., 2016; Shao et al., 2018; Wang et al., 2018; Wang et al., 2020). The combination of the two testing techniques can fully and accurately characterize the microstructure of loess and has been applied in the understanding of loess microstructure (Lei, 1987) and the analysis of the microstructure evolution of loess during shearing and collapsing (Jiang et al., 2014; Ng et al., 2016; Shao et al., 2018; Wang et al., 2018; Li et al., 2020; Wang et al., 2020). The water content of intact loess greatly influences its compressibility, but so far, the understanding remains insufficient, that is, the influence of water content on the microstructure of intact loess and the microstructure evolution during wetting and loading.

This article presents the results of oedometer tests performed on intact loess at different water contents, focusing on the evolution of the compressibility of intact loess under wetting and loading. To explore the mechanism of compression response, microstructures of intact loess specimens at different water contents before and after compression are characterized by SEM and MIP, which are compared and analyzed in terms of the evolution of the particle contact relation and PSD.

2 MATERIALS AND METHODS

2.1 Materials

Lanzhou is located in the northwest of the Loess Plateau in China, where thick loess distributes entirely in the sense of stratigraphy, and the three main stratigraphic units of loess are named Wucheng loess (Q_1), Lishi loess (Q_2), and Malan loess (Q_3). All loess samples were excavated by utilizing hand tools at a depth of 3–4 m below the slope top, which is the Malan loess and is yellow, as shown in **Figure 1A**. The excavated loess blocks were carefully cut into several 25-cm cubes and immediately sealed in

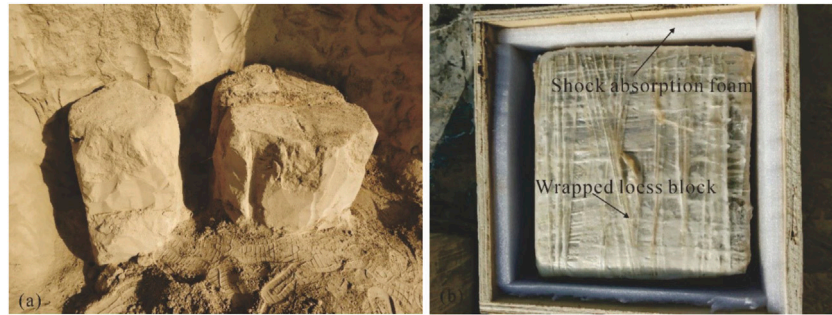


FIGURE 1 | Procedures of block samples: **(A)** trimming a block sample; **(B)** packing with a plastic membrane and preserving the sample in a wooden box.

TABLE 1 | Geotechnical characteristics of the studied loess.

Property	Value
Sample depth: m	3–4
Natural water content w : %	7.14
Natural degree of saturation S_r : %	20
Specific gravity G_s	2.78
Dry unit mass ρ_d : g/cm ³	1.396
Clay fraction (<5 μm): %	10.36
Silt fraction (5–75 μm): %	80.78
Sand fraction (>75 μm): %	8.86
Plastic limit w_p : %	17.9
Liquid limit w_l : %	29.7
Plasticity index I_p	11.8
Main minerals	
Quartz: %	40.2
Feldspar: %	22.9
Calcite: %	8.4
Dolomite: %	4.0
Hornblende: %	3.8
Illite: %	15.1
Chlorite: %	2.9
Others: %	2.7

cling film. They were then wrapped in a plastic membrane and coated with melted paraffin. Finally, the wrapped blocks were placed in specifically designed wooden boxes equipped with shock absorption foam on all inner sides, as shown in **Figure 1B**. These works were carried out on samples in order to preserve the natural water content as much as possible and minimize the disturbance during transportation.

Some basic physical properties of loess are summarized in **Table 1**. The intact loess is dry with a water content of 7.14% and a low dry density of 1.396 g/cm³. Based on the indoor tests, the specific gravity, liquid limit, and plastic limit of the studied loess were determined as 2.78, 29.7%, and 17.9%, respectively. The particle size distribution, as shown in **Figure 2**, was tested by the particle size analyzer Mastersizer 2000, which indicated that the loess dominantly comprises silt, accounting for 80.78%, and contains a small amount of clay (10.36%), which has a controlling effect on the mechanical behavior of loess (Cilek, 2001; Smalley and Marković, 2014; Li et al., 2016). The mineralogical composition of the loess was obtained by X-ray diffraction, which reveals that the loess consists mainly of non-clay minerals (quartz, albite, and

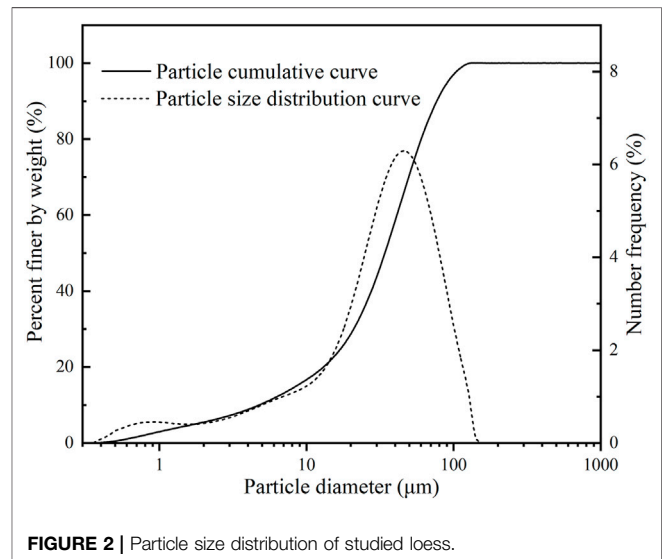


FIGURE 2 | Particle size distribution of studied loess.

calcite), accounting for more than 79%. Calcite (8.4%) in the soil needs to be focused on since some studies have shown that calcite is an essential component for enhancing the mechanical strength of loess (Wen and Yan, 2014; Meng and Li, 2019; Pihlap et al., 2021). In addition, loess also contains some clay minerals, mainly illite, accounting for 15.1%. The cementation effect of clay minerals and secondary calcite is an essential factor in the formation of the metastable structure of loess (Cilek, 2001; Smalley and Marković, 2014; Li et al., 2016; Liu et al., 2016).

2.2 Test Methods

2.2.1 Specimen Preparation

The specimens for oedometer tests were trimmed from the block sample with steel rings of 61.8 mm in diameter and 20 mm in height, which have a natural water content of 7.14%. The other specimens were wetted by adding distilled water onto the natural specimens to saturation degrees of 30%, 40%, 50%, 60%, 70%, 80%, and 90%. Saturated specimens were obtained by the vacuum saturation approach. The wetted specimens were wrapped in cling film and placed in a moisture chamber for 72 h in order to ensure the uniform distribution of water to the maximum extent. The initial state of each specimen is shown in **Table 2**.

TABLE 2 | Specimens of the oedometer test.

Test	Sample description	Initial state				Final state			
		e_0	ρ_{d0} (g/cm ³)	w_0 (%)	S_{r0} (%)	e_r	ρ_{dr} (g/cm ³)	w_r (%)	S_{rr} (%)
SL01	Natural state	0.992	1.396	7.14	20.01	0.749	1.589	7.03	26.09
SL02	Wetting	0.990	1.397	10.45	29.34	0.694	1.641	9.32	41.34
SL03	Wetting	0.992	1.396	13.91	38.97	0.648	1.687	11.76	59.03
SL04	Wetting	0.993	1.395	18.03	50.08	0.629	1.706	13.15	75.80
SL05	Wetting	0.987	1.399	21.19	59.68	0.624	1.712	17.34	77.25
SL06	Wetting	0.991	1.396	25.10	70.22	0.593	1.745	18.33	85.93
SL07	Wetting	0.993	1.395	28.64	80.17	0.576	1.764	18.84	90.93
SL08	Wetting	0.991	1.396	32.08	89.85	0.558	1.784	18.91	96.20
SL09	Vacuum saturation	0.993	1.395	35.02	98.03	0.532	1.815	18.98	99.18

2.2.2 Oedometer Test

Xie and Xing, (2016) concluded that the total amount of deformation of loess when it is wetted to certain water content under a certain pressure is independent of the stress path, the wetting path, and the sequence of loading and wetting; therefore, for a specific loess specimen, the pore ratio after wetting and compression is unique, and based on which, Shao et al. (2018) studied the wetting collapse characteristics of remolded loess. Similarly, this study simulates the evolution of loess compressibility during wetting by means of compression tests on specimens at different wetting stages. The specimens were first installed onto the oedometer boxes, a wetted cotton cloth was stuffed into the water tank of the box to reduce the evaporation of the unsaturated specimens, and the saturated specimen was filled with water in the water tank. Then, the axial displacement transducer was installed and checked if all parts were in contact. Finally, the data acquisition system was turned on and the loading process was initiated. The loading paths for each specimen were 12.5, 25, 50, 100, 200, 400, 800, 1,600, and 3,200 kPa. The compression test stability standard was 24 h after loading (Standardization Administration of China (SAC), Ministry of Water Resources, 2019). For secondary compression stability standard, the loading time was extended under each loading until axial deformation was less than 0.002 mm per day (Ge et al., 2015). After the test, the specimens were carefully taken out from the apparatus and freeze-dried for microstructure tests. The state of each specimen after compression is shown in **Table 2**.

2.2.3 Microstructure Test

The microstructure of intact loess due to wetting and the microstructure evolution of loess at different saturations after compressing were observed and compared using SEM and MIP, focusing on particle morphology, contact relation, bonding materials, and PSD. Five specimens were observed, including natural and saturated loess and after-compressed intact, 50% saturated and unsaturated loess, which were dried by the freezing method to reduce the damage to the microstructure during specimen preparation.

Cubic bars with the dimensions of 2 cm × 1 cm × 1 cm (length × width × height) were carefully trimmed off from the dried specimens and broken from the middle to reveal a fresh surface and coated with gold for SEM. A series of SEM images at different magnifications were taken for each sample to observe the morphology of the particle distribution and the details of the particle contact.

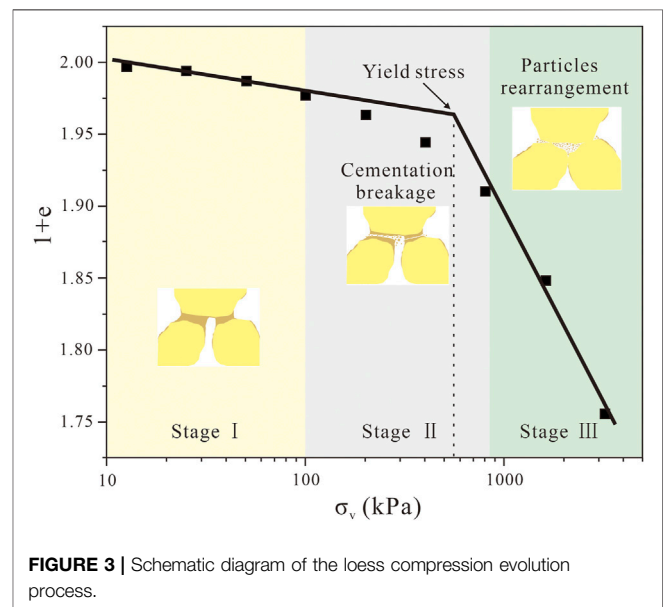


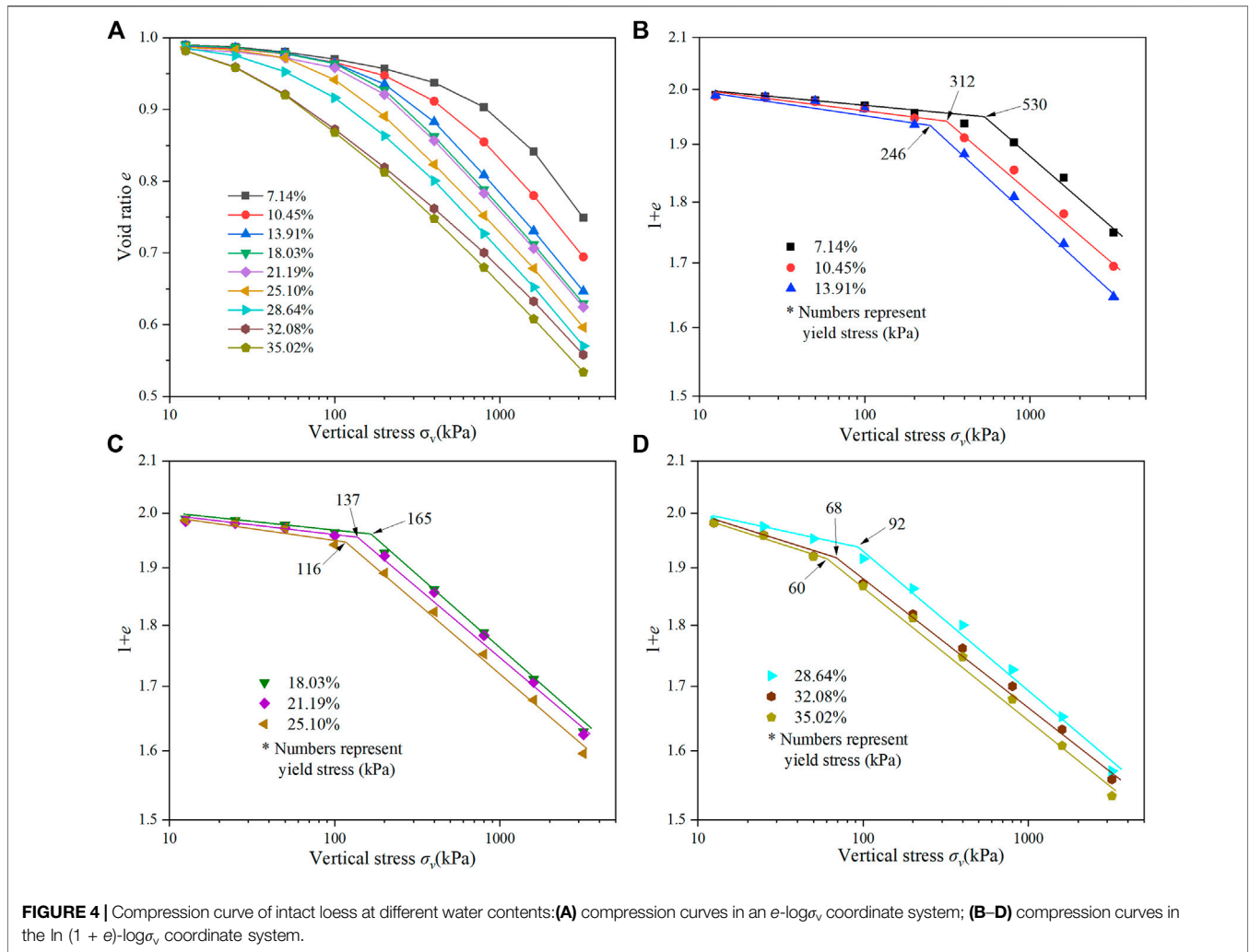
FIGURE 3 | Schematic diagram of the loess compression evolution process.

The samples of MIP were cubes with a side length of 1 cm, which were trimmed out from dried specimens same as that for SEM samples. Mercury is a non-wetting fluid that requires external pressure to intrude into the pore of soil, which progressively intrudes into tinier pores as the pressure increases, and the intrusion volume of mercury and intrusion pressure can be continuously monitored. A simplified assumption is that pores are cylindrical and the relationship between intrusion pressure and intruded pore diameter can be written as: $P = -4\gamma\cos\theta/D$, where P is the pressure that the mercury can intrude into the pore with the diameter of D , γ is the surface tension of mercury, and θ represents the contact angle of the mercury with the pore walls. In this article, $\gamma = 0.485\text{N/m}$, $\theta = 130^\circ$, and mercury intrusion pressure in MIP instrument ranges from 0.52 psi to 54955.09 psi.

3 RESULTS AND DISCUSSION

3.1 Evaluation of Compressibility

Benatti and Miguel (2013) proposed the structural models for colluvial and lateritic soil based on their three stages of collapsible



behavior, considering the effects of matrix suction and cementation. Analogously, intact loess has typical characteristics of unsaturated and intergranular cementation. **Figure 3** shows that the compression of loess can be divided into three stages in the $1+e\text{-}\log\sigma_v$ coordinate: (I) the skeleton particles become tighter, with a slight linear decrease in the void ratio at low vertical stress. (II) Interparticle cementations and aggregates gradually break, and overhead structure collapses, with decreasing void ratio at an increasing rate of change in void ratio at intermediate vertical stress. (III) Complete breakage of interparticle cementations and aggregates and particle rearrangement, with a sharp decrease in the void ratio at high vertical stress. However, these stages are not completely separated, for example, cementation breakage and particle movement are also observed in stage I, but only elastic compaction is predominant. A curved connection (Stage II) between two straight lines (stages I and III) indicates that interparticle cementation gradually fractures with increasing vertical pressure. In the $\ln(1+e)\text{-}\log\sigma_v$ plane, the pore ratio varies nearly linearly with increasing vertical pressure in the two phases of elastic compaction and particle rearrangement, and the

vertical pressure corresponding to the intersection of the two linear segments is determined as yield stress (Sridharan et al., 1991; Cheng et al., 2020; Leng et al., 2021).

Figure 4A shows the compression curves of intact loess at different initial water contents in the $e\text{-}\log\sigma_v$ plane. The void ratio of all specimens decreases with vertical stress; at the same initial pore ratio and higher initial water content, and the faster void ratio decreases. According to the method proposed by Sridharan et al. (1991), the yield stress values of intact loess at different initial water contents were determined, as shown in **Figures 4B–D**. When the water content of the specimens is low, the two straight sections are evident, as shown in **Figure 4B**. When the water content of the specimens is very high, the slope of the two straight lines is almost the same, as shown in **Figure 4D**. The intersection of the two lines gradually moves to the left as water content increases, that is, the higher the water content is, the smaller the yield stress of the intact loess. Yield stress decreases sharply and then stabilizes as water content increases, as shown in **Figure 5**, in which the relationship can be well-fitted by the power function based on initial water content w_0 . This result is consistent with the conclusion of other articles (Chen et al.,

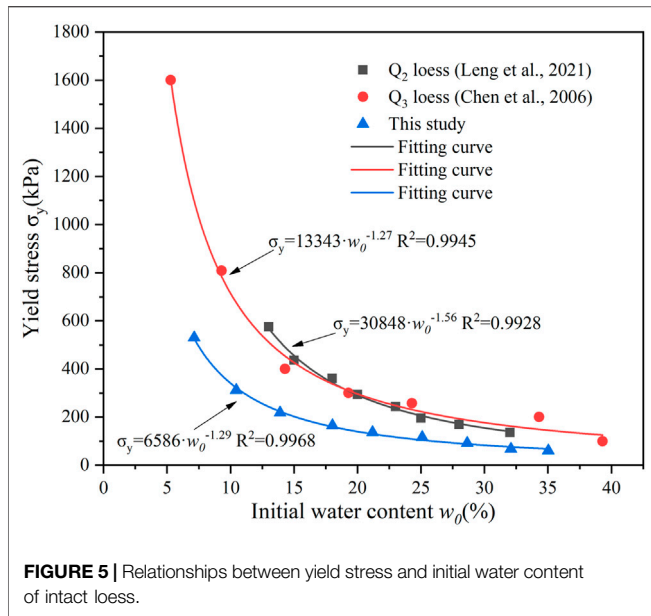


FIGURE 5 | Relationships between yield stress and initial water content of intact loess.

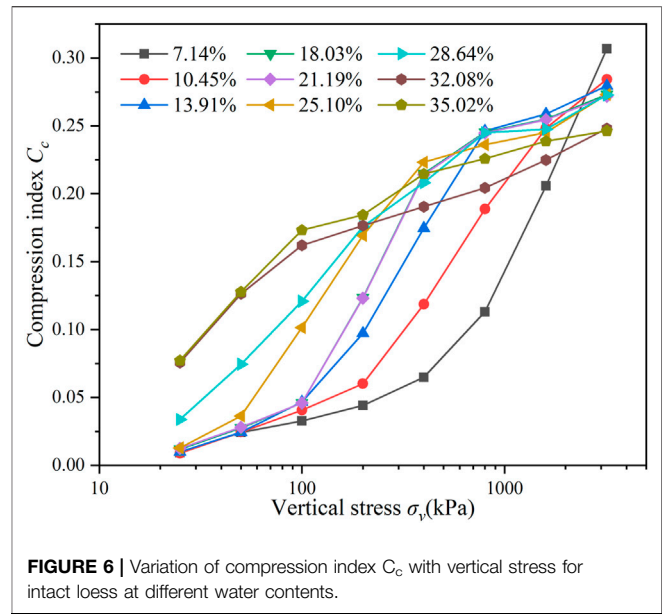


FIGURE 6 | Variation of compression index C_c with vertical stress for intact loess at different water contents.

2006; Leng et al., 2021), as presented in **Figure 5**. Moreover, the yield stress of intact loess is approximately 530 kPa, which is substantially higher than the overburden earth pressure, and some researchers (Muñoz-Castelblanco et al., 2012; Sadeghi et al., 2019) presumed that the apparent over-consolidation should be related to the soil-forming process, where cementation between skeletal particles provides great cohesion.

Compression index (C_c) is the slope of the compression curve that can be defined as $C_c = \Delta e / \Delta \log \sigma_v$, which evolves with vertical stress and is frequently used to evaluate the compressibility of soils. **Figure 6** shows the variation of compression index with vertical stress, and the compression index of each specimen increases with increasing vertical stress. However, the evolution of the compression index of specimens at different water contents follows different paths. The compression index of loess at low water content increases slowly and then sharply with vertical stress. By contrast, the compression index of loess with high water content is initially high and then increases gradually with vertical stress, but the variation rate gradually decreases. Further observation of the evolution of the compression index shows that the difference of the evolution path of the compression index seems related to yield stress. When the vertical stress exceeds yield stress, the compression index increases greatly. The evolution of the compression index with vertical stress is related to yield stress, which is similar in other soils (Arenaldi Perisic et al., 2019; Rezania et al., 2020). The further increase of compressibility at a low water content when vertical stress exceeds yield stress may arise from two aspects: on the one hand, the fracture of inter-particle cementation leads to sudden reduction in strength and a great deal of pore space remains after the previous loading; on the other hand, the increase in saturation due to volume compression contributes to the compressibility of unsaturated soil (Rezania et al., 2020). **Table 2** shows that although the water content of the specimen decreases after compression, the saturation increases.

3.2 Evaluation of Secondary Compressibility

The compression of soils consists of two stages: the primary compression stage, in which effective stress is increased with the extrusion of pore water and pore gas, resulting in the compression of soil volume, and the secondary compression stage, in which effective stress is constant, and the packing density of soil particles increases slowly with time (Mitchell and Soga, 2005). The study of the secondary compression characteristics of soils is of great importance in evaluating long-term stability, especially in loess areas of China. When evaluating the settlement deformation caused by long-term irrigation in the loess tableland, secondary compression deformation cannot be ignored.

The demarcation point of primary and secondary compression in the void ratio versus the logarithm of time (e -log t) is not easy to determine accurately and quickly. Mataic et al. (2016) suggested that secondary compression of soft clay soil occurs from the period of 6–24 h for each load increment; the summary of loess secondary compression shows that the time corresponding to the demarcation point of primary and secondary compression of loess gradually prolongs with the increase in vertical stress and is distributed within 46–200 min (Ge et al., 2015; Zhi et al., 2018). To reduce the complexity and subjective error of determining the demarcation point, this study considers that the secondary compression stage is the period from 200 min to the moment at which deformation stability occurs (vertical deformation is less than 0.002 mm per day). During this period, the void ratio decreases linearly with the logarithm of time, whose slope is defined as the secondary compression index and is usually expressed as $C_\alpha = \Delta e / \log(t_2/t_1)$, where t_1 is the time of the demarcation point of primary and secondary compression, t_2 is the time of deformation stability, and Δe is the change in the void ratio during the secondary compression stage.

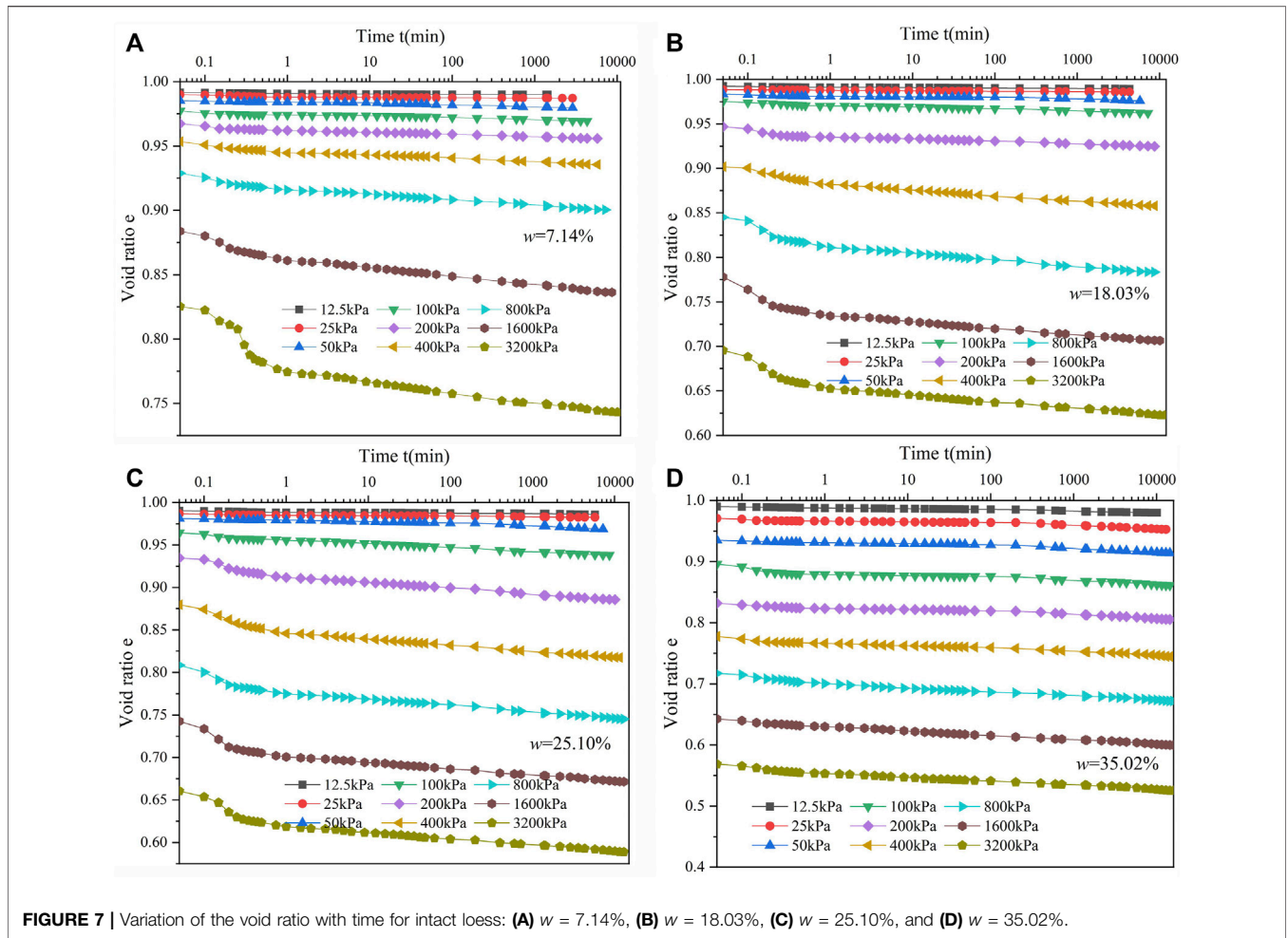


FIGURE 7 | Variation of the void ratio with time for intact loess: **(A)** $w = 7.14\%$, **(B)** $w = 18.03\%$, **(C)** $w = 25.10\%$, and **(D)** $w = 35.02\%$.

Figure 7 shows the variation in the void ratio with the logarithm of time for loess at different water contents, such as 7.14% (natural water content), 18.03%, 25.10%, and 35.02% (saturated). For all specimens, the void ratio decreases with time during each loading stage, and the variation rate is great at the beginning of loading stage and gradually slows down with time. Higher volume variations occur in the primary compression stage or secondary compression stage, with an increase in vertical stress, particularly when vertical stress is greater than yield stress.

Figure 8 illustrates the variation in the void ratio with the logarithm of time for specimens at different water contents under the same vertical stress. The secondary compression of loess increases with increase in water content at low vertical stress as shown in **Figure 8A**. However, with the increase in vertical stress, the secondary compression characteristics of loess at different water contents are similar. When $\sigma_v = 3,200$ kPa, the e -log t curves of each specimen in the secondary compression stage are parallel to one another, as shown in **Figure 8D**. The effect of water content on the secondary compression of loess is gradually weakened with increasing vertical stress. The water softens the bonding materials in loess (Wen and Yan, 2014), and for unsaturated soils, water menisci at the interparticle contacts apply tensile pressure to the skeleton particles for preventing

particle rearrangement (Rezania et al., 2020), which leads to increase in loess secondary compressibility with the increase in water content at low vertical stress. Interparticle cementation and suction hindered the development of secondary compression.

Figure 9A shows the variation curves of secondary compression index (C_{α}) with vertical stress for loess at different water contents. The secondary compression index of loess at low water contents increases with vertical stress, and the secondary compression index of loess at high water contents reaches the peak and then slightly decreases to a constant value with vertical stress, which is similar to the results of other literature (Arenaldi Perisic et al., 2019; Rezania et al., 2020). Comparison with the compression index curves (**Figure 6**) shows that they exhibit a similar variation pattern in the logarithmic of vertical stress. Many of the studies (Mesri and Castro, 1987; Zhang et al., 2007; Santagata et al., 2008; Carlos, 2018) concluded that C_{α}/C_c is a constant value which is independent of the stress level and specimen type (undisturbed or remodeled). However, some studies found a poor linear correlation between C_{α} and C_c . Zhang and Wang (2012) speculated that the structure of soft clay prevents its C_{α}/C_c from being a constant value. Mataic et al. (2016) found that the C_{α}/C_c value of Perniö clay increases with effective stress and then decreases and converges to a constant

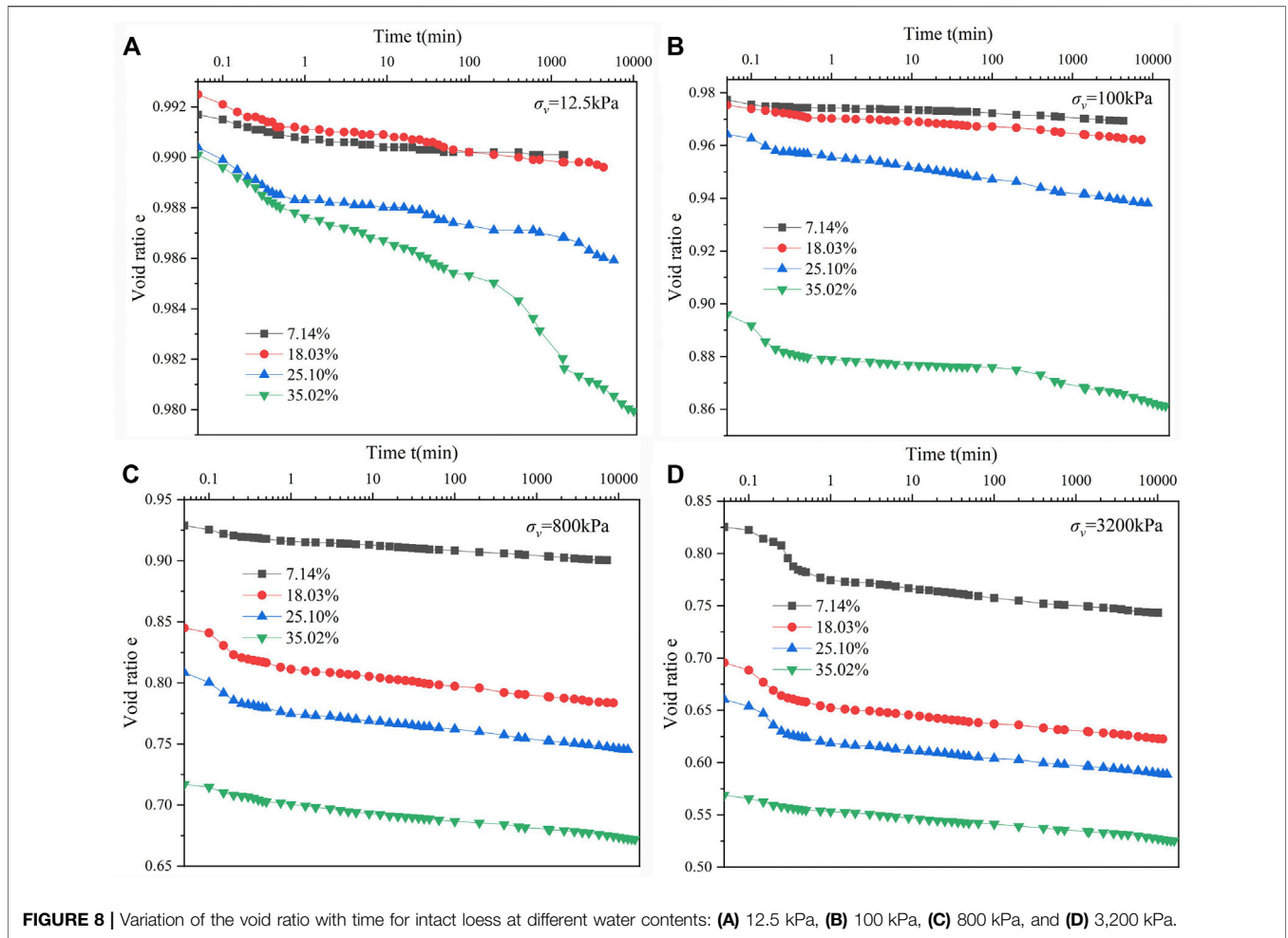


FIGURE 8 | Variation of the void ratio with time for intact loess at different water contents: (A) 12.5 kPa, (B) 100 kPa, (C) 800 kPa, and (D) 3,200 kPa.

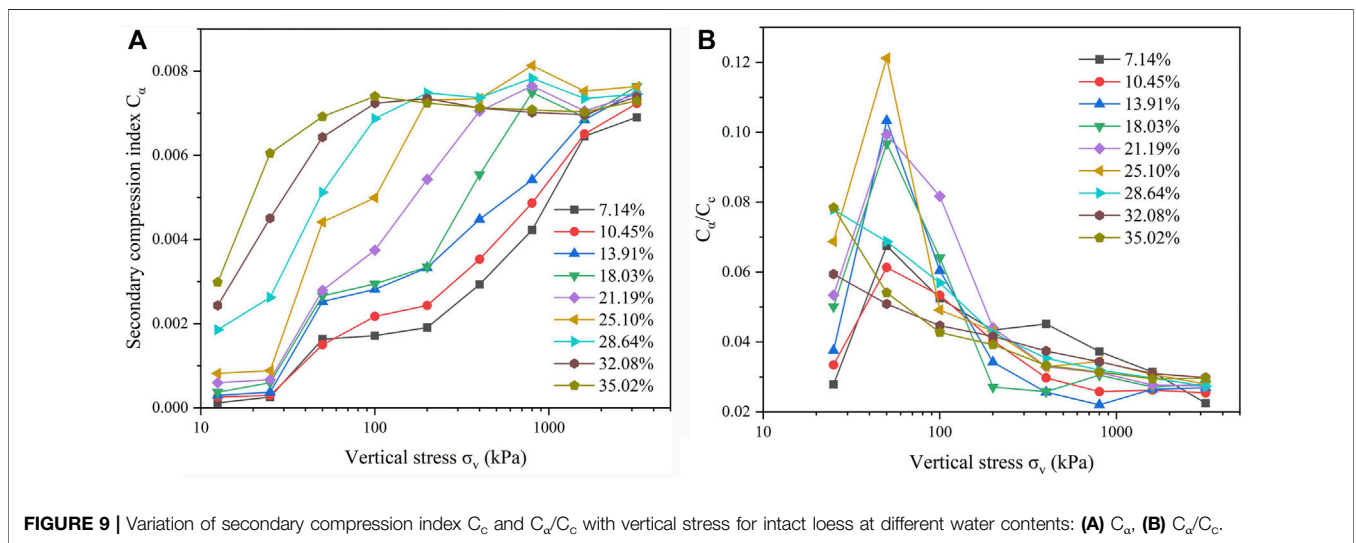


FIGURE 9 | Variation of secondary compression index C_c and C_{α}/C_c with vertical stress for intact loess at different water contents: (A) C_c , (B) C_{α}/C_c .

value (0.036). The C_{α}/C_c value at a low water content first increases with vertical stress to a peak and then gradually decreases and stabilizes as shown in **Figure 9B**, displaying a

similar variation pattern as the result of Perniö clay (Mataic et al., 2016). However, a slight difference is that the C_{α}/C_c value of loess at higher water content gradually decreases and stabilizes, and the

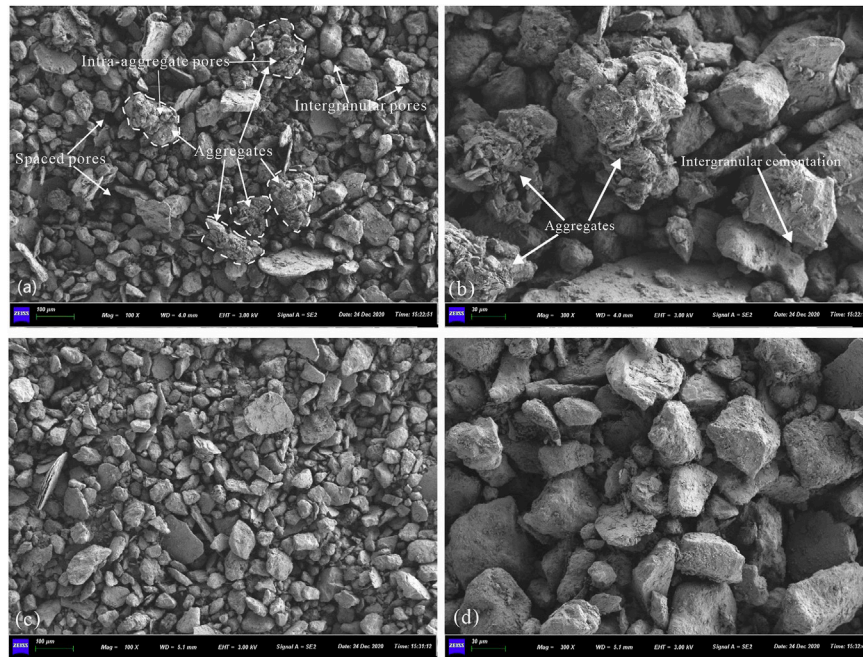


FIGURE 10 | Photomicrographs of intact loess and saturated loess. Overall view: **(A)** intact loess and **(C)** saturated loess; detailed view: **(B)** intact loess and **(D)** saturated loess.

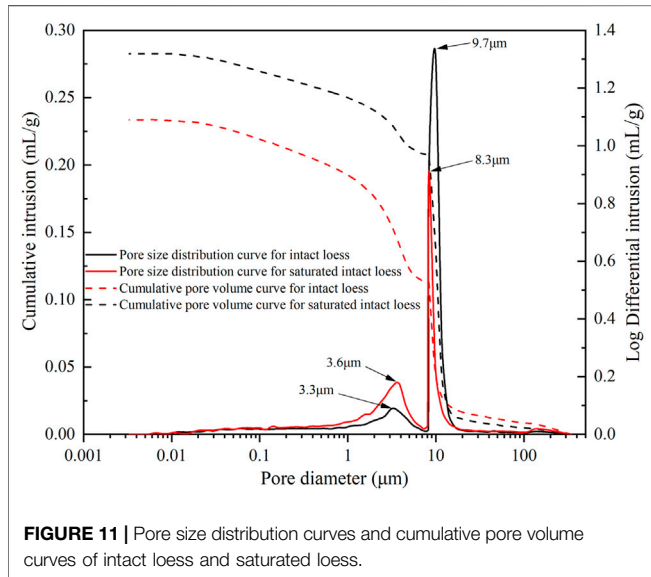


FIGURE 11 | Pore size distribution curves and cumulative pore volume curves of intact loess and saturated loess.

C_a/C_c values of all specimens eventually converge to around 0.025.

3.3 Microstructure Analyses

3.3.1 Microstructure and PSD of Intact and Saturated Loess

Figures 10A,B are the SEM images of intact loess, where the overall microstructure such as skeletal particles and pore distribution is observed at low-magnifications, and the surface

morphology of the particles, interparticle contact, and bonding material are observed at high magnifications. In addition to silt and sand, aggregates are an essential part of skeleton particles in intact loess, which are formed when a large number of clay particles clumped together on their own or when clay particles and carbonates bonded with silt (Gao, 1980a; Li et al., 2016; Liu et al., 2016; Pihlap et al., 2021). In the deposition, the skeleton particles are randomly and loosely arranged, making the loess form an opening metastable structure. The Lanzhou intact loess has the typical microstructure characteristics of loess: silt, sand, and aggregates are contacted point-to-point, and bonds at the contact are few, forming an overhead pore structure, as shown in Figure 10A. The cementation of clay and calcium carbonate in loess plays a vital role in the metastable structure (Cilek, 2001; Smalley and Marković, 2014; Li et al., 2016; Liu et al., 2016; Yates et al., 2018; Meng and Li., 2019). Figure 10B clearly shows that clay particles are distributed on the surface and contact point of skeleton particles, rather than emerging independently. Secondary calcium carbonate can occur due to the precipitation of carbonates (Pihlap et al., 2021), which reinforce the bonding structure and help trap clay particles at skeleton particle contacts (Smalley and Marković, 2014). Although observing the secondary calcium carbonate directly is difficult, some experiments showed that the strength of loess decreases evidently after the removal of calcium carbonate, which can prove the cementation effect of secondary calcium carbonate (Meng and Li, 2019). The high compressibility of intact loess and its sensitivity to water mainly come from the overhead structure and the softening effect of water on cementation materials, where high porosity provides space for compression deformation and

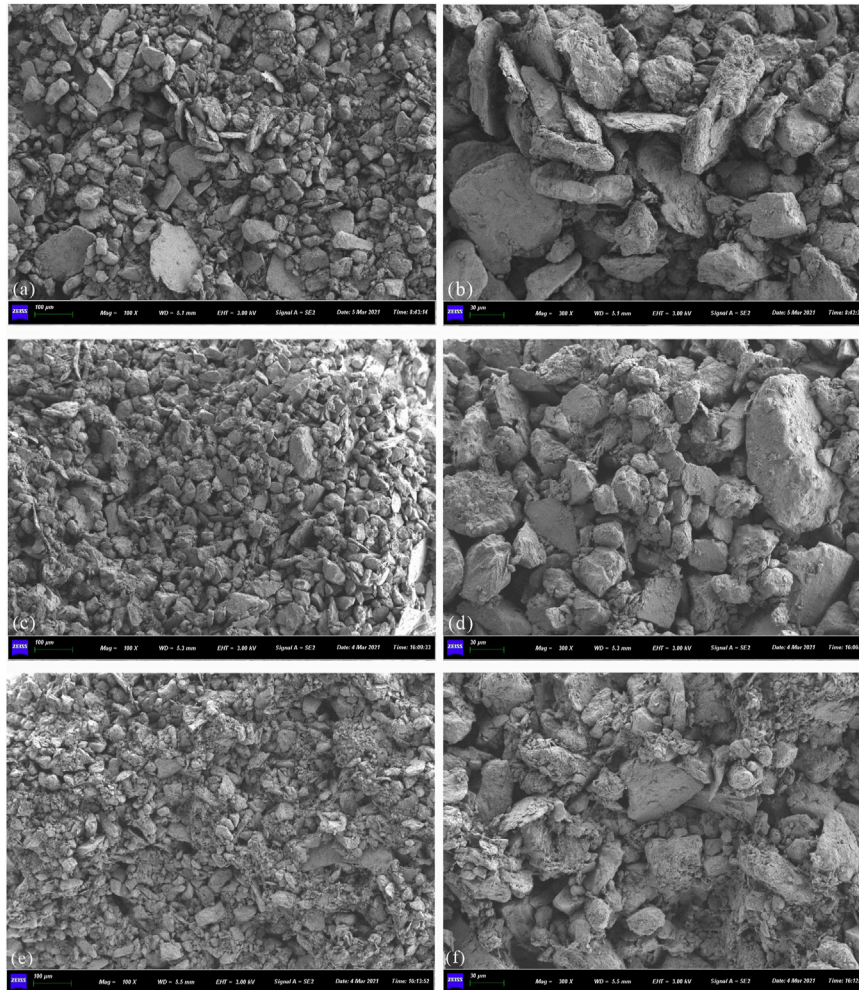
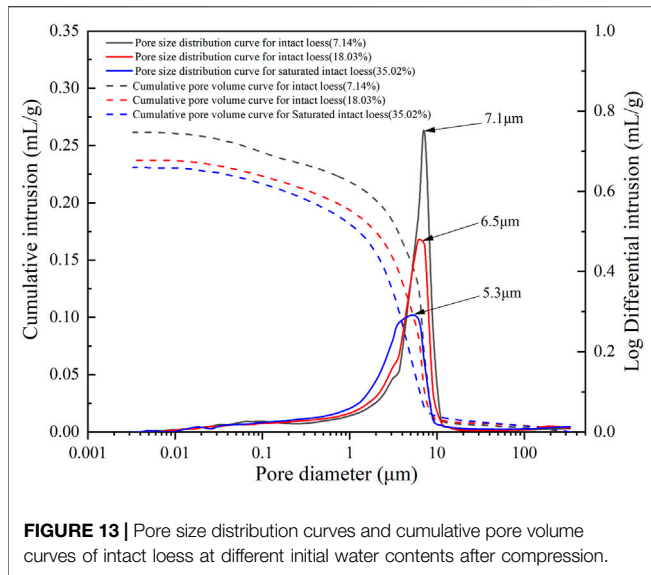


FIGURE 12 | Photomicrographs of intact loess at different initial water contents after compression: **(A,B)** overall view and detailed view, $w_0 = 7.14\%$; **(C,D)** overall view and detailed view, $w_0 = 18.03\%$; **(E,F)** overall view and detailed view, $w_0 = 35.02\%$.

the hydrophilicity of clay minerals makes the compressibility of loess extremely sensitive to the change in water content. The microstructure of saturated loess is shown in **Figures 10C,D**, which is still dominated by overhead structure, but when compared with intact loess, the distribution of skeleton particles and pores is more uniform, and the macropores are closed. The most remarkable phenomenon is the disappearance of the aggregates prevalent in intact loess after saturation.

MIP, which has been widely used in loess, has been proven to be one of the reliable methods to measure the PSD of soil (Ng et al., 2016; Wang et al., 2018). Lei (1987) divided pores of loess into four types according to pore radius: large pores ($>16\ \mu\text{m}$), mediate pores ($4\text{--}16\ \mu\text{m}$), small pores ($1\text{--}4\ \mu\text{m}$), and micropores ($<1\ \mu\text{m}$), which is referred to in this article. **Figure 11** shows the cumulative pore volume curves and pore size distribution curves of intact loess and saturated loess. The PSDs show two peaks in the intact loess and saturated loess, indicating two major pore groups in the loess structure. The first pore group with a dominant mediate

pore diameter is about $9.7\ \mu\text{m}$ for intact loess and about $8.3\ \mu\text{m}$ for saturated loess, and the second pore group with a small pore has a nearly identical diameter of about $3.5\ \mu\text{m}$ for intact and saturated loess, which indicates that mediate pore size of intact loess decreases slightly after saturation. The effect of inundation on pore structure of loess on the pore volume is remarkable. The cumulative intrusion pore volume of intact loess decreases from 0.28 to 0.23 after saturation, indicating that the overhead structure of intact loess collapses due to inundation. Moreover, in intact loess, mediate pore accounts for 69.38% of total pore volume and decreases to 41.31% after saturation, and small pores increase from 15.67% to 35.33%. Therefore, mediate pore collapses when loess is inundated, leading to transformation from mediate pores to small pores. In terms of total pore volume and pore size, inundation reconstructs the pore structure of loess and makes it more homogeneous, causing some damage to the original microstructure of intact loess.



3.3.2 Microstructure and PSD of Loess at Different Water Contents After Compression

Compression tests show that water content has a considerable influence on the compressibility of loess, and the damage of hydraulic effect on loess microstructure is analyzed. However, to reveal the evolution of loess compressibility under wetting and loading through the change of loess microstructure under hydro-mechanical effect, the microstructure changes of loess at different water contents after compression must be understood. Therefore, three after-compression samples of loess at different initial water contents are selected for SEM and MIP, namely, 7.14% (natural state), 18.03% (saturation 50.03%), and 35.03% (saturated state).

Figure 12 shows the microscopic images of loess at different water contents after compression. The microstructure of saturated loess drastically changes compared with others. For intact loess, as shown in **Figures 12A,B**, aggregates and intergranular cementation are destroyed under loading, overhead structures collapse, intergranular pores become smaller, and skeleton particles are in closer contact. However, it is still dominated by the point-to-point and point-to-face contact of skeleton particles and retains some microstructure characteristics of intact loess. Comparison between the microscopic images of the sample at natural water content, as shown in **Figure 12A**, and the microscopic images of samples at higher water contents, as shown in **Figures 12C, E**, suggests that skeleton particles are more homogeneously distributed and closely contacted with increasing water content. Comparing **Figure 12B** with **Figures 12D, F** shows that the microstructure changes from overhead structure to interlocking structure with the increase in water content. In summary, the microstructure of loess undergoes a radical transformation under the action of saturating and loading, and intact loess retains some original structure under high pressure and has the potential to further compress under wetting.

Figure 13 shows the PSD curves of loess at different initial water contents after compression. Compared with the cumulative intruded pore volume of the intact loess (**Figure 11**), compression leads to considerable reduction in the total pore volume of loess, and the reduction in pore volume decreases more with increasing water content. The PSD curves of the after-compressed specimens show a more substantial change from a bimodal peak to a unimodal peak compared with intact loess specimen, regardless of water content. Moreover, in response to an increase in water content, the height of the single peak decreases and the peak that defines the dominant pore diameter on the PSDs shifts to the left. Compression with high pressure cannot eliminate the collapsible pores of intact loess, and wetting can promote further collapse of mediate pores to form a more compact structure.

The evolution of microstructure and pore size distribution due to wetting and loading is consistent with the compression responses of intact loess. At low vertical stress, microstructure damage due to wetting is the key factor causing great difference in compressibility of loess. Under high vertical stress, intact loess retains some original microstructure, but microstructure damage is aggravated to form a compact interlocking structure due to wetting.

4 CONCLUSION

A series of oedometer tests were performed to investigate the compression characteristics of intact loess at different initial water contents. SEM and MIP tests were also carried out on specimens before and after compression to understand the evolution of microstructure and PSD during wetting and loading. The following conclusions can be drawn:

For intact loess, the increase in water content results in an increase in the slope of the compression curve and the values of secondary compression index and a decrease in yield stress. C_c and C_α increase with vertical stress. For intact loess, at low initial water content, the C_c values are very small and increase suddenly after vertical stress exceeds yield stress. For intact loess at high initial water content, C_c values increase sharply during the low loading stage, but the change gradually slows down with the increase in vertical stress. C_α shows a similar variation pattern in the logarithmic of vertical stress as the C_c . The C_α/C_c value of intact loess is dependent on water content and vertical stress and thus cannot be considered a constant value. However, it tends to be a constant value of about 0.025 at high vertical stress.

Intact loess has an overhead structure with loose arrangement and weak cementation of particles, and bimodal PSD is dominated by mediate and small pores. Inundating leads to collapse of aggregates and overhead structure and the transformation of mediate pores into small pores. After compression, the overhead structure of intact loess collapses, pore space decreases, and the bimodal peak of PSDs transforms into a unimodal peak. Compression at high pressure cannot drastically eliminate the collapsible pores of intact loess, and wetting can further make mediate pores collapse to form a more compact structure.

DATA AVAILABILITY STATEMENT

The original contributions presented in the study are included in the article/supplementary material; further inquiries can be directed to the corresponding author.

AUTHOR CONTRIBUTIONS

TJ: conceptualization, methodology, validation, data curation, and writing—original draft. LK: conceptualization,

methodology, and writing—review and editing. WB: conceptualization, methodology, and writing—review and editing. ZS: writing—review and editing.

FUNDING

This work was supported by the National Key R&D Program of China (Grant No. 2018YFC 1505304) and the National Natural Science Foundation of China (Nos. 41877281, 41772339).

REFERENCES

- Arenaldi Perisic, G., Ovalle, C., and Barrios, A. (2019). Compressibility and Creep of a Diatomaceous Soil. *Eng. Geol.* 258, 105145. doi:10.1016/j.enggeo.2019.105145
- Assallay, A. M., Rogers, C. D. F., and Smalley, I. J. (1997). Formation and Collapse of Metastable Particle Packings and Open Structures in Loess Deposits. *Eng. Geol.* 48, 101–115. doi:10.1016/s0013-7952(97)81916-3
- Bally, R. J. (1988). Some Specific Problems of Wetted Loessial Soils in Civil Engineering. *Eng. Geol.* 25 (2-4), 303–324. doi:10.1016/0013-7952(88)90034-8
- Barden, L., McGown, A., and Collins, K. (1973). The Collapse Mechanism in Partly Saturated Soil. *Eng. Geol.* 7 (1), 49–60. doi:10.1016/0013-7952(73)90006-9
- Benatti, J. C. B., and Miguel, M. G. (2013). A Proposal of Structural Models for Colluvial and Lateritic Soil Profile from Southwestern Brazil on the Basis of Their Collapsible Behavior. *Eng. Geol.* 153, 1–11. doi:10.1016/j.enggeo.2012.11.003
- Carlos, O. (2018). On the Role of Particle Breakage in Primary and Secondary Compression of Wet and Dry Sand. *Geotech. Lett.* 8 (2), 1–15. doi:10.1680/jgele.18.00047
- Chen, C. L., Hu, Z. Q., and Gao, P. (2006). Research on Relationship between Structure and Deformation Property of Intact Loess. *Chin J Rock Soil Mech* 11, 1891–1896. (in Chinese). doi:10.3321/j.issn:1000-6915.2006.07.009
- Cheng, Q., Zhou, C., Ng, C. W. W., and Tang, C. S. (2020). Effects of Soil Structure on Thermal Softening of Yield Stress. *Eng. Geol.* 269, 105544. doi:10.1016/j.enggeo.2020.105544
- Cilek, V. (2001). The Loess Deposits of the Bohemian Massif: Silt Provenance, Palaeometeorology and Loessification Processes. *Quat. Int.* 76-77, 123–128. doi:10.1016/s1040-6182(00)00096-3
- Dijkstra, T. A., Smalley, I. J., and Rogers, C. D. F. (1995). Particle Packing in Loess Deposits and the Problem of Structure Collapse and Hydroconsolidation. *Eng. Geol.* 40, 49–64. doi:10.1016/0013-7952(95)00022-4
- Francisca, F. M. (2007). Evaluating the Constrained Modulus and Collapsibility of Loess from Standard Penetration Test. *Int. J. Geomech.* 7 (4), 307–310. doi:10.1061/(asce)1532-3641(2007)7:4(307)
- Gao, G. R. (1980b). Classification for Microstructure of Loess and its Collapsibility. *Sci. Sin.* 12, 1203–1208. (in Chinese).
- Gao, G. R. (1988). Formation and Development of the Structure of Collapsing Loess in China. *Eng. Geol.* 25 (2-4), 235–245. doi:10.1016/0013-7952(88)90029-4
- Gao, G. R. (1980a). The Microstructure of Loess in China. *Chin. Sci. Bull.* 20, 945–948. (in Chinese).
- Ge, M. M., Li, N., Zheng, J. G., Zhu, C. H., and Bai, Y. Y. (2015). Prediction of the Post-construction Settlement of High Filled Embankment with Considering the Time Depending Deformation of Compacted Loess. *Chin. Civ. Eng. J.* 48 (S2), 262–267. (in Chinese).
- Grabowska-Olszewska, B. (1989). Skeletal Microstructure of Loesses - its Significance for Engineering-Geological and Geotechnical Studies. *Appl. Clay Sci.* 4 (4), 327–336. doi:10.1016/0169-1317(89)90040-9
- Handy, R. L. (1973). Collapsible Loess in Iowa. *Soil Sci. Soc. Am. J.* 37 (2), 281–284. doi:10.2136/sssaj1973.03615995003700020033x
- Hou, X., Vanapalli, S. K., and Li, T. (2018). Water Infiltration Characteristics in Loess Associated with Irrigation Activities and its Influence on the Slope Stability in Heifangtai Loess Highland, China. *Eng. Geol.* 234, 27–37. doi:10.1016/j.enggeo.2017.12.020
- Hou, X., Vanapalli, S. K., and Li, T. (2019). Wetting-induced Collapse Behavior Associated with Infiltration: A Case Study. *Eng. Geol.* 258, 105146. doi:10.1016/j.enggeo.2019.105146
- Jiang, M., Hu, H., and Liu, F. (2012). Summary of Collapsible Behaviour of Artificially Structured Loess in Oedometer and Triaxial Wetting Tests. *Can. Geotech. J.* 49 (10), 1147–1157. doi:10.1139/t2012-075
- Jiang, M., Zhang, F., Hu, H., Cui, Y., and Peng, J. (2014). Structural Characterization of Natural Loess and Remolded Loess under Triaxial Tests. *Eng. Geol.* 181, 249–260. doi:10.1016/j.enggeo.2014.07.021
- Juang, C. H., Dijkstra, T., Wasowski, J., and Meng, X. (2019). Loess Geohazards Research in China: Advances and Challenges for Mega Engineering Projects. *Eng. Geol.* 251, 1–10. doi:10.1016/j.enggeo.2019.01.019
- Lei, X. Y. (1987). Pore Types of the Loess in China and its Collapsibility. *Sci. Sin.* 12, 1309–1318. (in Chinese).
- Leng, Y., Peng, J., Wang, Q., Meng, Z., and Huang, W. (2018). A Fluidized Landslide Occurred in the Loess Plateau: A Study on Loess Landslide in South Jingyang Tableland. *Eng. Geol.* 236, 129–136. doi:10.1016/j.enggeo.2017.05.006
- Leng, Y., Peng, J., Wang, S., and Lu, F. (2021). Development of Water Sensitivity Index of Loess from its Mechanical Properties. *Eng. Geol.* 280 (3), 105918. doi:10.1016/j.enggeo.2020.105918
- Li, P., Vanapalli, S., and Li, T. L. (2016). Review of Collapse Triggering Mechanism of Collapsible Soils Due to Wetting. *J. Rock Mech. Geotech.* 8 (02), 256–274. doi:10.1016/j.jrmge.2015.12.002
- Li, P., Shao, S., and Vanapalli, S. K. (2020). Characterizing and Modeling the Pore-Size Distribution Evolution of a Compacted Loess during Consolidation and Shearing. *J. Soils Sediments* 20 (7), 2855–2867. doi:10.1007/s11368-020-02621-3
- Li, X.-A., Li, L., Song, Y., Hong, B., Wang, L., and Sun, J. (2019). Characterization of the Mechanisms Underlying Loess Collapsibility for Land-Creation Project in Shaanxi Province, China—a Study from a Micro Perspective. *Eng. Geol.* 249, 77–88. doi:10.1016/j.enggeo.2018.12.024
- Li, X. A., and Li, L. (2017). Quantification of the Pore Structures of Malan Loess and the Effects on Loess Permeability and Environmental Significance, Shaanxi Province, China: an Experimental Study. *Environ. Earth Sci.* 76 (15), 523. doi:10.1007/s12665-017-6855-7
- Liu, T. S. (1985). *Loess and Environment*. Beijing: Science Press, 1–481. (in Chinese).
- Liu, Z., Liu, F., Ma, F., Wang, M., Bai, X., Zheng, Y., et al. (2016). Collapsibility, Composition, and Microstructure of Loess in China. *Can. Geotech. J.* 53, 673–686. doi:10.1139/cgj-2015-0285
- Lu, Q., Qiao, J., Peng, J., Liu, Z., Liu, C., Tian, L., et al. (2019). A Typical Earth Fissure Resulting from Loess Collapse on the Loess Plateau in the Weihe Basin, China. *Eng. Geol.* 259, 105189. doi:10.1016/j.enggeo.2019.105189
- Mataic, I., Wang, D. X., and Korkiala-Tanttu, L. (2016). Effect of Destructuration on the Compressibility of Pernio Clay in Incremental Loading Oedometer Tests. *Int. J. Geomech.* 16 (1), 040150161. doi:10.1061/(asce)gm.1943-5622.0000486
- Meng, J., and Li, X.-A. (2019). Effects of Carbonate on the Structure and Properties of Loess and the Corresponding Mechanism: an Experimental Study of the Malan Loess, Xi'an Area, China. *Bull. Eng. Geol. Environ.* 78 (7), 4965–4976. doi:10.1007/s10064-018-01457-z
- Mesri, G., and Castro, A. (1987). Ca/Cc Concept and K₀ during Secondary Compression. *J. Geotech. Engrg.* 113, 230–247. doi:10.1061/(asce)0733-9410(1987)113:3(230)

- Mitchell, J. K., and Soga, K. (2005). *Fundamentals of Soil Behaviour*. 3rd ed. New Jersey: John Wiley & Sons, 353–355.
- Muñoz-Castelblanco, J. A., Delage, P., Pereira, J. M., and Cui, Y. J. (2012). On-sample Water Content Measurement for a Complete Local Monitoring in Triaxial Testing of Unsaturated Soils. *Géotechnique* 62 (7), 595–604. doi:10.1680/geot.10.p.129
- Ng, C. W. W., Sadeghi, H., Hossen, S. K. B., Chiu, C. F., Alonso, E. E., and Baghbanrezvan, S. (2016). Water Retention and Volumetric Characteristics of Intact and Re-compacted Loess. *Can. Geotech. J.* 53, 1258–1269. doi:10.1139/cgj-2015-0364
- Nouaouria, M. S., Guenfoud, M., and Laffi, B. (2008). Engineering Properties of Loess in Algeria. *Eng. Geol.* 99 (1–2), 85–90. doi:10.1016/j.enggeo.2008.01.013
- Pihlap, E., Steffens, M., and Kögel-Knabner, I. (2021). Initial Soil Aggregate Formation and Stabilisation in Soils Developed from Calcareous Loess. *Geoderma* 385, 114854. doi:10.1016/j.geoderma.2020.114854
- Rezania, M., Bagheri, M., and Mousavi Nezhad, M. (2020). Creep and Consolidation of a Stiff Clay under Saturated and Unsaturated Conditions. *Can. Geotech. J.* 57, 728–741. doi:10.1139/cgj-2018-0398
- Reznik, Y. M. (1992). Determination of Deformation Properties of Collapsible Soils. *Geotech. Test. J.* 15 (3), 248–255.
- Sadeghi, H., Kiani, M., Sadeghi, M., and Jafarzadeh, F. (2019). Geotechnical Characterization and Collapsibility of a Natural Dispersive Loess. *Eng. Geol.* 250, 89–100. doi:10.1016/j.enggeo.2019.01.015
- Santagata, M., Bobet, A., Johnston, C. T., and Hwang, J. (2008). One-dimensional Compression Behavior of a Soil with High Organic Matter Content. *J. Geotech. Geoenviron. Eng.* 134 (1), 1–13. doi:10.1061/(asce)1090-0241(2008)134:1(1)
- Saye, S. R., Nass, K. H., and Easton, C. N. (1988). Performance of Heavy Structures Founded upon Loess at Varying Moisture Conditions. *Eng. Geol.* 25 (2–4), 325–339. doi:10.1016/0013-7952(88)90035-x
- Shao, S. J., Li, J., Li, G. L., Deng, G. H., Zhang, J.-W., Liu, Y., et al. (2015). Evaluation Method for Self-Weight Collapsible Deformation of Large Thickness Loess Foundation. *Chin. J. Geotech. Eng.* 6, 965–978. (in Chinese). doi:10.11779/CJGE201506001
- Shao, X., Zhang, H., and Tan, Y. (2018). Collapse Behavior and Microstructural Alteration of Remolded Loess under Graded Wetting Tests. *Eng. Geol.* 233, 11–22. doi:10.1016/j.enggeo.2017.11.025
- Smalley, I. J., and Marković, S. B. (2014). Loessification and Hydroconsolidation: There Is a Connection. *Catena* 117, 94–99. doi:10.1016/j.catena.2013.07.006
- Sridharan, A., Abraham, B. M., and Jose, B. T. (1991). Improved Technique for Estimation of Preconsolidation Pressure. *Géotechnique* 41 (2), 263–268. doi:10.1680/geot.1991.41.2.263
- Standardization Administration of China (SAC), Ministry of Water Resources (2019). *China National Standards GB/T50123-2019: Standard for Soil Test Method*. Beijing: China Planning Press. (in Chinese).
- Wang, J.-D., Li, P., Ma, Y., and Vanapalli, S. K. (2018). Evolution of Pore-Size Distribution of Intact Loess and Remolded Loess Due to Consolidation. *J. Soils Sediments* 19 (3), 1226–1238. doi:10.1007/s11368-018-2136-7
- Wang, J.-D., Li, P., Ma, Y., Vanapalli, S. K., and Wang, X.-G. (2020). Change in Pore-Size Distribution of Collapsible Loess Due to Loading and Inundating. *Acta Geotech.* 15 (5), 1081–1094. doi:10.1007/s11440-019-00815-9
- Wen, B.-P., and Yan, Y.-J. (2014). Influence of Structure on Shear Characteristics of the Unsaturated Loess in Lanzhou, China. *Eng. Geol.* 168, 46–58. doi:10.1016/j.enggeo.2013.10.023
- Xie, D. Y., and Xing, Y. C. (2016). *Soil Mechanics for Loess Soils*. Beijing: Higher Education Press, 37–50. (in Chinese).
- Xie, W.-L., Li, P., Vanapalli, S. K., and Wang, J.-D. (2018). Prediction of the Wetting-Induced Collapse Behaviour Using the Soil-Water Characteristic Curve. *J. Asian Earth Sci.* 151, 259–268. doi:10.1016/j.jseas.2017.11.009
- Xu, L., Dai, F., Tu, X., Tham, L. G., Zhou, Y., and Iqbal, J. (2014). Landslides in a Loess Platform, North-West China. *Landslides* 11 (6), 993–1005. doi:10.1007/s10346-013-0445-x
- Yang, Y. S., Li, J., Xing, Y. C., and Zhao, J. M. (2017). Experimental Study on Moistening Deformation Characteristics of Compacted Loess and Their Influencing Factors. *Chin. J. Geotech. Eng.* 39 (04), 626–635. (in Chinese). doi:10.11779/CJGE201704006
- Yates, K., Fenton, C. H., and Bell, D. H. (2018). A Review of the Geotechnical Characteristics of Loess and Loess-Derived Soils from Canterbury, South Island, New Zealand. *Eng. Geol.* 236, 11–21. doi:10.1016/j.enggeo.2017.08.001
- Youssef, A. M., and Maerz, N. H. (2013). Overview of Some Geological Hazards in the Saudi Arabia. *Environ. Earth Sci.* 70 (7), 3115–3130. doi:10.1007/s12665-013-2373-4
- Zhang, W. B., Xie, Y. L., and Yang, X. H. (2007). Research on 1D Secondary Consolidation Characteristics of Compacted Loess. *Chin. J. Geotech. Eng.* 29 (05), 765–768. (in Chinese). doi:10.3321/j.issn:1000-4548.2007.05.022
- Zhang, W., Sun, Y., Chen, W., Song, Y., and Zhang, J. (2019). Collapsibility, Composition, and Microfabric of the Coastal Zone Loess Around the Bohai Sea, China. *Eng. Geol.* 257, 105142. doi:10.1016/j.enggeo.2019.05.019
- Zhang, X. W., and Wang, C. M. (2012). Effect of Soft Clay Structure on Secondary Consolidation Coefficient. *Chin J Rock Soil Mech* 33 (02), 479–482. (in Chinese). doi:10.3969/j.issn.1000-7598.2012.02.025
- Zhi, B., Wang, P., Wang, Y. X., Wu, L., and Jiao, H. (2018). Study on Properties of Secondary Consolidation of Structured Loess under High Fill. *Chin. J. Eng. Geol.* 26 (6), 1447–1453. (in Chinese). doi:10.13544/j.cnki.jeg.2017-415

Conflict of Interest: The authors declare that the research was conducted in the absence of any commercial or financial relationships that could be construed as a potential conflict of interest.

Publisher's Note: All claims expressed in this article are solely those of the authors and do not necessarily represent those of their affiliated organizations, or those of the publisher, the editors, and the reviewers. Any product that may be evaluated in this article, or claim that may be made by its manufacturer, is not guaranteed or endorsed by the publisher.

Copyright © 2022 Jian, Kong, Bai and Sun. This is an open-access article distributed under the terms of the Creative Commons Attribution License (CC BY). The use, distribution or reproduction in other forums is permitted, provided the original author(s) and the copyright owner(s) are credited and that the original publication in this journal is cited, in accordance with accepted academic practice. No use, distribution or reproduction is permitted which does not comply with these terms.